PHYSICAL REVIEW D **87,** 053001 (2013)

Higgs boson and top quark masses as tests of electroweak vacuum stability

Isabella Masina[1,2]

[1]*Dipartimento di Fisica dell'Università di Ferrara and INFN Sezione di Ferrara, Via Saragat 1, I-44100 Ferrara, Italy*
[2]*CP*^{3}*—Origins and DIAS, Southern Denmark University, Campusvej 55, DK-5230 Odense M, Denmark*
(Received 16 October 2012; published 6 March 2013)

The measurements of the Higgs boson and top-quark masses can be used to extrapolate the Standard Model Higgs potential at energies up to the Planck scale. Adopting a next-to-next-to-leading-order renormalization procedure, we (i) find that electroweak vacuum stability is at present allowed and discuss the associated theoretical and experimental errors and the prospects for its future tests, (ii) determine the boundary conditions allowing for the existence of a shallow false minimum slightly below the Planck scale, which is a stable configuration that might have been relevant for primordial inflation, and (iii) derive a conservative upper bound on type-I seesaw right-handed neutrino masses, following from the requirement of electroweak vacuum stability.

DOI: 10.1103/PhysRevD.87.053001 PACS numbers: 14.80.Bn, 11.10.Gh, 13.15.+g

I. INTRODUCTION

The recent discovery of a particle consistent with the Standard Model (SM) Higgs boson, announced by the ATLAS [1] and CMS [2] collaborations at CERN, is a milestone in particle physics; adding in quadrature statistical and systematic errors, the mass of the particle turns out to be in the range 124.8–126.5 GeV at 2σ.

Here we assume that the new particle is actually the SM Higgs boson and study the implications that its mass value—together with other relevant parameters, such as the top-quark mass and the strong gauge coupling—has on the behavior of the Higgs potential at very high energy scales and, in particular, for the sake of electroweak vacuum stability.

The project of extrapolating the Higgs potential up to the Planck scale is a long-standing one [3–5], and was revamped in the fall of 2011 [6–9] after the first LHC hints of a Higgs boson were reported [10]. Recently, the tools for a next-to-next-to-leading-order (NNLO) renormalization procedure were derived [11–14]. So there are now all the ingredients necessary to carry out this long-standing project. Clearly, the extrapolation is based on the assumption that there is a desert up to the Planck scale or, better, that possible new physics do not significantly affect the running of the Higgs quartic coupling, which dominates the Higgs potential at high energy.

It is interesting that the recently discovered experimental Higgs mass range, combined with the experimental top mass range, indicates a particularly intriguing high-energy behavior of the Higgs potential close to the transition between electroweak vacuum stability and metastability. This is due to the fact that, for these Higgs and top mass values, the Higgs quartic coupling can be very small or even negative. Since the dependence on the top mass is strong and quite subtle, it is not surprising that different groups slightly disagree in the interpretation of the results, some of them favoring [13] and others disfavoring [14] electroweak vacuum stability.

Traditionally, the top pole mass was used in the analysis; however, it has been pointed out [15] that the top pole mass value used in previous analyses and taken to be the one measured at the Tevatron, $m_t^{\rm exp} = 173.2 \pm 0.9$ GeV [16], is not unambiguously derived, and that a more careful derivation should be based instead on the running top mass in the $\overline{\rm MS}$ scheme, $\bar{m}_t(m_t) = 163.3 \pm 2.7$ GeV. As was shown in Ref. [15], the top pole mass range consistently derived from the running one, $m_t = 173.3 \pm 2.8$ GeV, is plagued by a larger error than the Tevatron measurement considered in Ref. [14], rescuing electroweak vacuum stability.

In our analysis we keep as a free parameter the running top mass, rather than the pole one. In this way we completely avoid the theoretical uncertainties associated with the top Yukawa matching procedure. As we are going to discuss, the theoretical error associated with the Higgs quartic coupling matching [13,14] turns out to be smaller than the one induced by the experimental uncertainty in the strong gauge coupling, $\alpha_3(m_Z)$. Given the above-mentioned range for the running top mass [15], we find that electroweak stability is allowed in the whole Higgs mass range [1,2]. Stability could soon be excluded if values of the running top mass $\bar{m}_t(m_t) < 163$ GeV are excluded by the LHC. Otherwise, testing electroweak vacuum stability would become very challenging, since this would require precision measurements of the Higgs and top masses, and also of $\alpha_3(m_Z)$.

A stable Higgs potential configuration which deserves particular interest is a shallow false minimum close to the Planck scale, which could have been relevant for primordial inflation [7,17,18]. We show that such a configuration is realized only if the Higgs quartic coupling and its derivative satisfy very specific boundary conditions, possibly having a deep origin in quantum gravity.

As is well known, new physics in addition to the SM is required to explain the neutrino masses and mixings, as well as dark matter. The mechanism responsible for the

neutrino masses could affect the Higgs quartic coupling; as an example, we consider the impact that the inclusion of neutrino masses via a type-I seesaw has on electroweak stability, discussing in some detail the shallow false minimum configuration.

The paper is organized as follows. In Sec. II we discuss the input parameters and the NNLO renormalization procedure used to extrapolate the Higgs potential up to the Planck scale. An analysis of electroweak vacuum stability and the associated constraints on the top and Higgs masses, with a detailed discussion of the theoretical errors and the prospects for the future, are presented in Sec. III. In Sec. IV we investigate the boundary conditions leading to the particularly interesting configuration of a shallow false minimum below the Planck scale. Section V is devoted to the upper bound on the seesaw right-handed neutrino masses following from the requirement of electroweak vacuum stability. Conclusions are drawn in Sec. VI. Appendix A contains the relevant formulas for the NNLO running procedure in the SM, and those needed to incorporate the type-I seesaw mechanism are found in Appendix B.

II. INPUT PARAMETERS AND RENORMALIZATION AT NNLO

The normalization of the Higgs quartic coupling λ is chosen in this paper so that the potential for the physical Higgs ϕ_H contained in the Higgs doublet $H = (0, (\phi_H + v)/\sqrt{2})$ is given, at tree level, by

$$V(\phi_H) = \frac{\lambda}{6}\left(|H|^2 - \frac{v^2}{2}\right)^2 \approx \frac{\lambda}{24}\phi_H^4, \tag{1}$$

where $v = 1/(\sqrt{2}G_\mu)^{1/2} = 246.221$ GeV and $G_\mu = 1.1663787(6) \times 10^{-5}/\text{GeV}^2$ is the Fermi constant from muon decay [19]. The approximation in Eq. (1) holds when considering large field values. According to our normalization, the physical Higgs mass satisfies the tree-level relation $m_H^2 = \lambda v^2/3$. In addition, the mass of the fermion f reads, at tree level, $m_f = h_f v/\sqrt{2}$, where h_f denotes the associated Yukawa coupling.

In order to extrapolate the behavior of the Higgs potential at very high energies, we adopt the $\overline{\text{MS}}$ scheme and consider the renormalization group (RG) evolution for the relevant couplings which, in addition to the Higgs quartic coupling λ, are the gauge g, g', g_3, and the top Yukawa h_t couplings. We work at NNLO, namely three-loops for the β functions and two-loops for the matching conditions at some suitable scale.

It is customary to introduce the dimensionless parameter $t = \log \mu/m_Z$, where μ stands for the renormalization scale and m_Z is the Z-boson mass. The RG equations for the relevant couplings are then given by

$$\begin{aligned}
\frac{d}{dt}\lambda(t) &= \kappa\beta_\lambda^{(1)} + \kappa^2\beta_\lambda^{(2)} + \kappa^3\beta_\lambda^{(3)},\\
\frac{d}{dt}h_t(t) &= \kappa\beta_{h_t}^{(1)} + \kappa^2\beta_{h_t}^{(2)} + \kappa^3\beta_{h_t}^{(3)},\\
\frac{d}{dt}g(t) &= \kappa\beta_g^{(1)} + \kappa^2\beta_g^{(2)} + \kappa^3\beta_g^{(3)},\\
\frac{d}{dt}g'(t) &= \kappa\beta_{g'}^{(1)} + \kappa^2\beta_{g'}^{(2)} + \kappa^3\beta_{g'}^{(3)},\\
\frac{d}{dt}g_3(t) &= \kappa\beta_{g_3}^{(1)} + \kappa^2\beta_{g_3}^{(2)} + \kappa^3\beta_{g_3}^{(3)},
\end{aligned} \tag{2}$$

where $\kappa = 1/(16\pi^2)$ and the apex on the β functions represents the loop order. The one-loop and two-loop expressions for the β functions can be found, e.g., in Ref. [20] (see also Refs. [21–26]). Recently, the complete three-loop β functions for all the SM gauge couplings have been presented by Mihaila, Salomon, and Steinhauser in Ref. [11], while the leading three-loop terms in the RG evolution of λ, h_t, and the Higgs anomalous dimension have been computed by Chetyrkin and Zoller in Ref. [12]. For the sake of completeness, the expressions for the β functions up to three loops are collected in Appendix A.

The matching of the running gauge couplings is done at the Z-boson pole mass,[1] m_Z. The numerical values used for the related $\overline{\text{MS}}$ observables are taken from the latest Particle Data Group SM fit results [19],

$$\begin{aligned}
\alpha_{\text{em}}^{-1}(m_Z) &= 127.944 \pm 0.014,\\
\alpha_3(m_Z) &= 0.1196 \pm 0.0017,\\
\sin^2\theta_W(m_Z) &= 0.23116 \pm 0.00012,\\
m_Z &= 91.1874 \pm 0.0021 \text{ GeV}.
\end{aligned} \tag{3}$$

To match the $\overline{\text{MS}}$ running quartic coupling $\lambda(\mu)$ with the Higgs pole mass m_H is more complicated and requires one to exploit the expansion

$$\begin{aligned}
\lambda(\mu) &= \sum_{n=1,2,3,\ldots} \lambda^{(n)}(\mu)\\
&= 3\frac{m_H^2}{v^2}(1 + \delta_H^{(1)}(\mu) + \delta_H^{(2)}(\mu) + \cdots),
\end{aligned} \tag{4}$$

which is known at present at NLO: $\delta_H^{(1)}(\mu)$ is the one-loop $\mathcal{O}(\alpha)$ result of Sirlin and Zucchini [27] while $\delta_H^{(2)}(\mu)$ is the recently calculated two-loop result, composed of a QCD contribution of $\mathcal{O}(\alpha\alpha_3)$ [13,14] and a Yukawa contribution [14]. More details can be found in Appendix A. As is well known, there is some arbitrariness in the choice of the matching scale μ in Eq. (4), which introduces a "theoretical" error in the RG procedure. In this work, we choose to perform the matching of the Higgs quartic

[1]We use the value of the strong coupling at m_Z and immediately apply the six-flavor running. The correction that would result by running with five flavors up to the top mass is very small and can be neglected, as was discussed in Ref. [13].

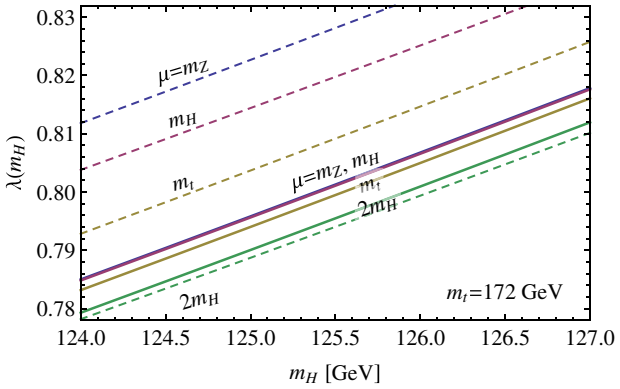

FIG. 1 (color online). Value of $\lambda(m_H)$ obtained by performing the matching at different scales μ—indicated by the labels—as a function of m_H. The solid (dashed) lines are obtained by including corrections up to the two-loop (one-loop) level. We fixed $m_t = 172$ GeV [for different values see Eq. (5)].

coupling λ at the scale $\mu = m_H$. The theoretical uncertainty is estimated by also performing the matching at different scales and by evolving λ via RG running until $\mu = m_H$. The spread in the numerical values obtained for $\lambda(m_H)$ can then be used to infer the magnitude of the theoretical error.

This is illustrated in Fig. 1, assuming for definiteness a top pole mass $m_t = 172$ GeV. The dashed and solid curves show the value of $\lambda(m_H)$ obtained by including the corrections up to the one-loop and two-loop levels, respectively, for various choices of the matching scale: from top to bottom, $\mu = m_Z, m_H, m_t, 2m_H$. One can see that, working at the one-loop level, the theoretical uncertainty is about 5%. The inclusion of the two-loop corrections given in Ref. [14] reduces the theoretical uncertainty to about 0.7%. Notice also that the preferred region shrinks to small λ values and that $\mu = m_Z$ and $\mu = m_H$ nearly overlap. More generally, one can use the following expression for the two-loop result:

$$\lambda(m_H) = 0.8065 + 0.0109(m_H[\text{GeV}] - 126) + 0.0015(m_t[\text{GeV}] - 172)^{+0.0002}_{-0.0060}, \quad (5)$$

where the mean value refers to $\mu = m_H$. The reference values of m_H and m_t used in Eq. (5) are not the central values that will be used in the following analysis; they are just "round numbers" that allow for an easy inspection of the variation of $\lambda(m_H)$ as a function of m_H and m_t.

Notice that it is not possible to directly compare Eq. (5) with Eq. (63) of Ref. [14], where $\lambda(m_t)$ is used instead (as well as the adoption of a normalization differing from ours by a factor of 6 and the use of the central values of m_H and m_t as reference values): $\lambda(m_t) = 0.12577 + 0.00205(m_H[\text{GeV}] - 125) - 0.0004(m_t[\text{GeV}] - 173.15) \pm 0.00140$, where the error is obtained by varying the matching scale between m_Z, m_t, and $2m_t$ [14]. We checked that our numerical code gives a result for $\lambda(m_t)$ consistent with that of Eq. (63) of Ref. [14]. Indeed, choosing $m_H = 125$ GeV and $m_t = 173.15$ GeV, our code gives $\lambda(m_t)/6 = 0.12605, 0.12575, 0.12412 = 0.12575^{+.0003}_{-.0016}$, when the matching scale $\mu = m_Z$, m_t, $2m_t$, respectively. This shows that the two results perfectly agree for $\mu = m_t$: the lower errors (associated with the difference between $\mu = m_t$ and $\mu = 2m_t$) are in substantial agreement, while the upper errors (associated with the difference between $\mu = m_Z$ and $\mu = m_t$) are slightly different, with ours being smaller.

It is common to extrapolate the $\overline{\text{MS}}$ top Yukawa coupling $h_t(\mu)$ from the matching condition between the running top mass $\bar{m}_t(\mu)$ and the top pole mass m_t,

$$h_t(\mu)\frac{v}{\sqrt{2}} = \bar{m}_t(\mu) = m_t(1 + \delta_t(\mu)),$$
$$\delta_t(\mu) = \delta_t^{\text{W}}(\mu) + \delta_t^{\text{QED}}(\mu) + \delta_t^{\text{QCD}}(\mu), \quad (6)$$

where $\delta_t^{\text{W}} + \delta_t^{\text{QED}}$ represent the electroweak contribution, which is known at the one-loop level [28], while δ_t^{QCD} is the QCD contribution. The QCD one-loop result has been known for many years [28]; the QCD two-loop and three-loop results as a function of the matching scale μ are given in Ref. [29] (see also Refs. [30–34]). The matching is usually done at the top pole mass scale, and the theoretical error associated with the arbitrariness of the matching scale can be estimated as before, namely by comparing the values of $h_t(m_t)$ obtained with different matching scales. This is represented in Fig. 2, where the curves are obtained by working at the two-loop level and using, from bottom to top, $\mu = m_Z$, m_t, $2m_t$. The plot shows that the associated theoretical uncertainty is about 2%. The analytical expression for $h_t(m_t)$ is

$$h_t(m_t) = 0.933 + 0.006(m_t[\text{GeV}] - 172)^{+0.017}_{-0.013}. \quad (7)$$

The variations of $h(m_t)$ due to the experimental range of α_s and m_H have not been explicitly written in Eq. (7) because they are negligible (of order 10% and 1%, respectively) with respect to the variation of $h(m_t)$ due to the experimental range of m_t. The error quoted in Eq. (7) then refers only to the

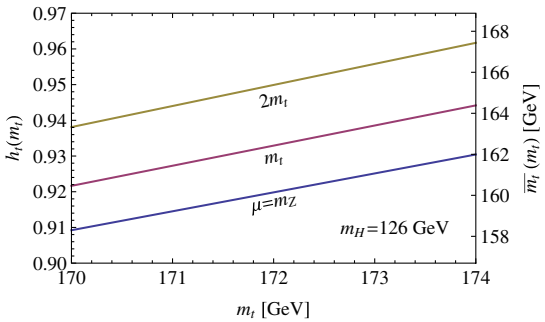

FIG. 2 (color online). Values of $h_t(m_t)$ and $\bar{m}_t(m_t)$ as a function of m_t. The curves are obtained by matching at different scales, which are indicated by the labels. We fixed $m_H = 126$ GeV for definiteness but the results do not significantly dependent on m_H, provided it is chosen in its experimental range.

theoretical error coming from varying the matching scale μ from m_Z, m_t (mean value), and $2m_t$. Notice that our result perfectly agrees with the analogous expression derived in Ref. [14], where (however) the error due to the variation of the matching was not estimated.

The procedure adopted in previous analyses of the stability of the electroweak vacuum, including the latest ones [13,14], was to use the experimental value of m_t—identified with the one measured at the Tevatron by the CDF and D0 collaborations, $m_t^{\rm exp} = 173.2 \pm 0.9$ GeV [16]—to extrapolate the running Yukawa $h_t(m_t)$ via Eq. (7). However, as discussed in Ref. [15], it is not meaningful to use the mass parameter provided by the Tevatron as the top pole mass to be inserted in Eq. (7): the running top mass in the $\overline{\rm MS}$ scheme is instead a well-defined parameter that can be directly extracted at NNLO from Tevatron measurements of the inclusive top pair production cross section, giving $\bar{m}_t(m_t) = 163.3 \pm 2.7$ GeV [15]. So, it is conceptually more robust and practically more convenient to extract the top Yukawa coupling directly from $\bar{m}_t(m_t)$, as will be done in the following.[2] Our results will thus be presented as a function of $\bar{m}_t(m_t)$.

Notice that, according to Eq. (7), the value of the top pole mass can be easily recovered via the relation $m_t = \bar{m}_t(m_t) + 9.6^{+2.9}_{-2.3}$ GeV, which, however, is plagued by a large uncertainty. In Ref. [15] it was found that, by doing a scheme transformation to NNLO accuracy from the running to the top pole mass, the range $\bar{m}_t(m_t) = 163.3 \pm 2.7$ GeV is equivalent to $m_t = 173.3 \pm 2.8$ GeV. Hence, while displaying our results as a function of $\bar{m}_t(m_t)$ (as already stated), and motivated by the results of Ref. [15], in some plots (such as Fig. 5) we will link the value of the top pole mass to the running mass via the simple relation $m_t = \bar{m}_t(m_t) + 10$ GeV.

Before presenting the results of our analysis in the following sections, we recall that, in order to carefully study the shape of the Higgs potential at high energy, one should consider the renormalization-improved effective potential. This can be done by introducing an effective coupling, $\lambda_{\rm eff}(\mu) = \lambda(\mu) + \Delta\lambda(\mu)$, so that

$$V_{\rm eff}(\phi_H) = \frac{\lambda_{\rm eff}(\mu)}{24}\,\phi_H^4. \tag{8}$$

The expression for $\Delta\lambda(\mu)$ is known up to the two-loop level [4,20] (and is given, for instance, in Ref. [14]). Since the scalar contribution is not well defined when λ is negative (a logarithm of a negative quantity appears), in the following we consider the renormalization-improved potential at the tree level, and identify μ with ϕ_H. It is well known that this simplification has a negligible impact on the determination of the vacuum stability bound (for a detailed discussion see, e.g., Ref. [13]), which will be discussed in the next section.

[2]In contrast, Ref. [15] proceeds in a more complicated way: the value of $\bar{m}_t(m_t)$ is translated into a value of m_t, which is inserted into the expression of the lower bound on m_H, ensuring electroweak vacuum stability as derived in Ref. [14].

III. ELECTROWEAK VACUUM STABILITY

The experimental region of the values of the Higgs and top masses is very intriguing from the theoretical point of view, since the Higgs quartic coupling could be rather small, vanish, or even turn negative at a scale slightly smaller than the Planck scale. Accordingly, the behavior of the Higgs potential at high energy changes drastically: if $\lambda(\mu)$ is always positive, the electroweak vacuum is a global minimum, possibly accompanied by another local minimum just below the Planck scale, which could have played a role in primordial inflation [7,17,18]; if $\lambda(\mu)$ turns negative below $M_{\rm Pl}$, the electroweak vacuum correspondingly becomes metastable [4,5].

These drastically different possibilities for the behavior of the renormalization-improved Higgs potential at high energy are illustrated in the left plot Fig. 3, where $m_H = 126$ GeV and some specific values for $\bar{m}_t(m_t)$ have been selected, increasing from top to bottom. The right plot shows the associated values of $\lambda(\mu)$. We start by considering the value $\bar{m}_t(m_t) = 161.989$ GeV. Increasing the latter by just 1 MeV, the potential develops an inflection point; notice that the associated $\lambda(\mu)$ becomes as small as $\mathcal{O}(10^{-5})$. Increasing $\bar{m}_t(m_t)$ again by about 200 keV, the minimum of $\lambda(\mu)$ is equal to zero: a second vacuum degenerate with the electroweak one is obtained. Increasing $\bar{m}_t(m_t)$ further makes $\lambda(\mu)$ turn negative: the electroweak vacuum becomes metastable.

The dashed curve in the right plot in Fig. 3 shows the evolution of $\beta_\lambda(\mu) = d\lambda(\mu)/dt$ for the same parameter values; there is only a single dashed curve because $\beta_\lambda(\mu)$ mildly depends on $\bar{m}_t(m_t)$ if the latter is in the range 161–163 GeV. We call μ_β the renormalization scale, such that $\beta_\lambda(\mu_\beta) = 0$. Clearly, only in the case of two degenerate vacua are the conditions $\beta_\lambda(\mu_\beta) = 0$ and $\lambda(\mu_\beta) = 0$ simultaneously met. For a shallow false minimum we instead have $\beta_\lambda(\mu_\beta) = 0$ and $\lambda(\mu_\beta) = \mathcal{O}(10^{-5})$, as already mentioned.

In Fig. 4 we show how μ_β depends on $\bar{m}_t(m_t)$, for various values of m_H. It is interesting that μ_β is maximized and nearly constant for the values of $\bar{m}_t(m_t)$ for which $\lambda(\mu)$ is very small.

We now turn to the determination of the points in the plane $[m_H, \bar{m}_t(m_t)]$ allowing for the existence of a second minimum degenerate with the electroweak one. These points belong to a line separating the stability from the metastability region; see Fig. 5. In the lower part of the plot $\lambda(\mu)$ is always positive, while in the upper part it becomes negative before reaching the Planck scale. The configuration of a shallow false minimum belongs to the stability region, but the associated points are so close to the transition line that they could not be distinguished visually.

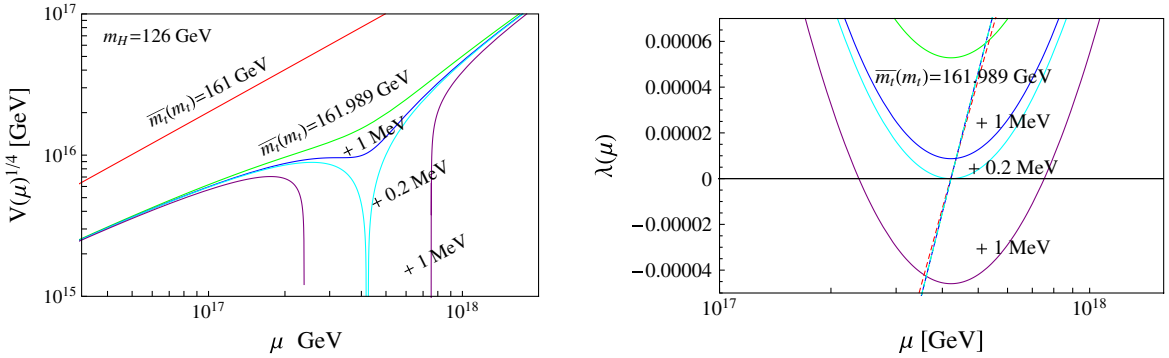

FIG. 3 (color online). The SM Higgs potential (left) and the quartic Higgs coupling (right) as functions of the renormalization scale μ, for $m_H = 126$ GeV and different values of $\bar{m}_t(m_t)$, increasing from top to bottom by the amount indicated by the labels. The dashed curve in the right plot shows the associated value of $\beta_\lambda(\mu)$. The other input parameters are fixed at the central values discussed in the previous section.

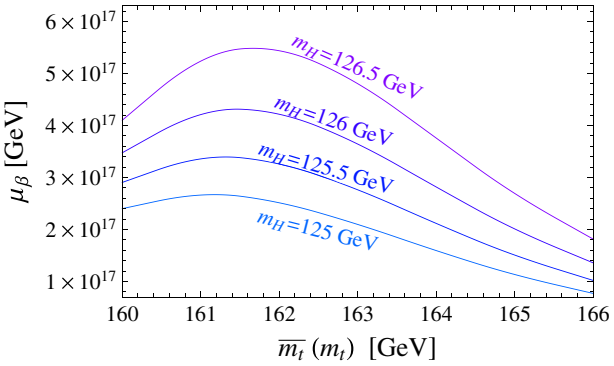

FIG. 4 (color online). The scale μ_β as a function of $\bar{m}_t(m_t)$ and for different values of m_H, as indicated by the labels.

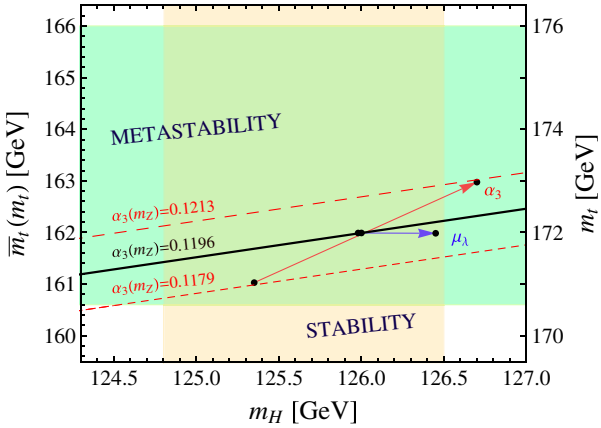

FIG. 5 (color online). The solid (black) line marks the points in the plane $[m_H, \bar{m}_t(m_t)]$ where a second vacuum, degenerate with the electroweak one, is obtained just below the Planck scale. The (red) diagonal arrow shows the effect of varying $\alpha_3(m_Z) = 0.1196 \pm 0.0017$ [19]; the (blue) horizontal arrow shows the effect of varying μ_λ (the matching scale of λ) from m_Z up to $2m_H$. The shaded (yellow) vertical region is the 2σ ATLAS [1] and CMS [2] combined range, $m_H = 125.65 \pm 0.85$ GeV; the shaded (green) horizontal region is the range $\bar{m}_t(m_t) = 163.3 \pm 2.7$ GeV, equivalent to $m_t = 173.3 \pm 2.8$ GeV [15].

The transition line of Fig. 5 was obtained with the input parameter values discussed in the previous section and by matching the running Higgs quartic coupling at m_H. Clearly, it is also important to estimate the theoretical error associated with the experimental ranges of the input parameters and the one associated with the matching procedure. To illustrate this, we consider in particular the point on the transition line associated with the value $m_H = 126$ GeV; for such a point, λ and β_λ both vanish at a certain scale μ_β (see Fig. 4). The arrows show how, if some inputs or the matching scale are changed, the position of this point must change in order to maintain, at the same scale μ_β, a vacuum degenerate with the electroweak one. The diagonal arrow is obtained by varying the strong coupling in its allowed range, $\alpha_3(m_Z) = 0.1196 \pm 0.0017$ [19]; the short (long) dashed line shows how the solid line would move if $\alpha_3(m_Z)$ were equal to its minimum (maximum) presently allowed value. Notice that the error on $\alpha_3(m_Z)$ induces an uncertainty in both the Higgs and top masses of about ± 0.7 GeV. In Ref. [14] the impact of the variation of $\alpha_3(m_Z)$ on m_H was estimated to be ± 0.5 GeV (see their Table 1). The two results are in substantial agreement, considering that in our analysis $\alpha_3(m_Z) = 0.1196 \pm 0.0017$ at 1σ [19], while Ref. [14] considers a smaller error, $\alpha_3(m_Z) = 0.1184 \pm 0.0007$ at 1σ. Since the variation of the other input parameters in Eq. (4) induces much smaller effects than the one due to $\alpha_3(m_Z)$, they have not been reported in Fig. 5. The horizontal arrow represents instead the theoretical error obtained by varying μ_λ, the matching scale of the Higgs quartic coupling, from $\mu = m_Z$ to $\mu = 2m_H$ (notice that the associated error is very asymmetric; see Fig. 1): essentially, it can only enhance m_H by at most 0.5 GeV. Clearly, similar considerations apply to each point of the transition line. We note that in Ref. [14] the impact of the variation of the matching scale of λ on m_H was estimated to be ± 0.7 GeV (see their Table 1), and hence close to our estimate but with a symmetric error.

Figure 5 shows that stability can be achieved in the whole experimental range for m_H (shaded vertical region),

but this is not the case for $\bar{m}_t(m_t)$ (shaded horizontal region). So, it is convenient to write down the condition of electroweak vacuum stability in the form of an upper bound on the running top mass,

$$\bar{m}_t(m_t)[\mathrm{GeV}] \leq 162.0 + 0.47(m_H[\mathrm{GeV}] - 126) + 0.7\left(\frac{\alpha_3(m_Z) - 0.1196}{0.0017}\right) - 0.2^{(\mu_\lambda)}_{\mathrm{th}}, \quad (9)$$

where the last term accounts for the (very asymmetric) theoretical error induced by the matching of λ. The latter turns out to be smaller than the variation induced by varying $\alpha_3(m_Z)$ in its presently allowed experimental range. We recall that the relation between the running and top pole mass is simply $m_t = \bar{m}_t(m_t) + 10$ GeV. Figure 6 summarizes our results for the determination of the transition line between stability and metastability in the $[m_H, m_t]$ plane. The three lines correspond to the central and $\pm 1\sigma$ values of $\alpha_3(m_Z)$ [19] and their thickness represents the theoretical error due to the matching of λ. The shaded rectangle emphasizes the present allowed region for m_t [15] and m_H [1,2]. According to our analysis it is not possible, given the present experimental situation, to understand whether we live in a stable or metastable vacuum configuration.[3]

In order to discriminate between the two possibilities, it would be crucial to better determine $\bar{m}_t(m_t)$. As discussed in Ref. [15], after LHC the Higgs mass will presumably be known with an accuracy of $\mathcal{O}(100)$ MeV [35], but the precision on the top mass would improve only by a factor of 2. For instance, if the whole range of $\bar{m}_t(m_t) < 163$ GeV (or, equivalently, $m_t < 173$ GeV) were excluded, we would conclude that our vacuum is metastable; otherwise the investigations should continue.

A self-consistent and precise determination of the top-quark mass can best be performed at a high-energy electron-positron collider, with a planned accuracy of $\mathcal{O}(100)$ MeV. Moreover, at an electron-positron collider $\alpha_3(m_Z)$ could be determined with an accuracy close to or better than $\Delta\alpha_3(m_Z) = 0.0007$ (this precision is sometimes currently adopted [13,14], but cannot be considered to be conservative according to Ref. [15]). At this stage, if the stability region will still have an overlap with the allowed ranges of the top and Higgs masses, we will be mostly limited by the theoretical uncertainty associated with μ_λ. Notice also that it is not realistic to hope to distinguish the case of two degenerate minima with that of a shallow false minimum, since the difference in the top mass is just about 200 keV (see Fig. 3).

We now discuss how to compare Eq. (9) and Fig. 6 with previous literature results, in particular those of Ref. [14], since the authors claimed that "absolute stability of the Higgs potential is excluded at 98% C.L. for $m_H < 126$ GeV" (see also their Fig. 5). In the latter work the stability condition is indeed expressed under the form of a lower bound on the Higgs mass: $m_H \geq 129.4 + 1.4(m_t - 173.1)/0.7 - 0.5(\alpha_3(m_Z) - 0.1184)/0.0007 \pm 1_{\mathrm{th}}$, where all masses are in GeV and the last term represents the overall theoretical error. Combining in quadrature their theoretical uncertainty and their experimental errors on m_t and $\alpha_3(m_Z)$, the authors derive $m_H > 129.4 \pm 1.8$ GeV, which motivates the quoted claim of Ref. [14]. In order to carry out the comparison, one must rewrite the inequality of Ref. [14] under a form directly comparable with Eq. (9), namely

$$m_t^{[14]}[\mathrm{GeV}] \leq 171.8 + 0.5(m_H[\mathrm{GeV}] - 126) + 0.61\left(\frac{\alpha_3(m_Z) - 0.1196}{0.0017}\right) \pm 0.5_{\mathrm{th}}. \quad (10)$$

So, our results (9) and those obtained in Ref. [14] are perfectly compatible, as the central value of Eq. (10) essentially overlaps with the lower value of Eq. (9). The theoretical error in Eq. (9) is however smaller than the theoretical error of Ref. [14]; this is mainly due to the fact that in the present analysis we used the running top mass directly, thus avoiding the need to introduce the theoretical error due to the matching scale of the top Yukawa coupling (see Table 1 of Ref. [14]). The left plot of Fig. 7 shows the comparison between Eqs. (9) and (10) in the determination of the transition line between stability and metastability in the $[m_H, m_t]$ plane; we choose $\alpha_3(m_Z) = 0.1196$ for definiteness, so that the thickness of the lines represent just the theoretical error. According to Eq. (9) the thickness of the line is 0.2 GeV, while according to Eq. (10) it is 1 GeV (as can also be checked by inspecting Table 1 of Ref. [14]).

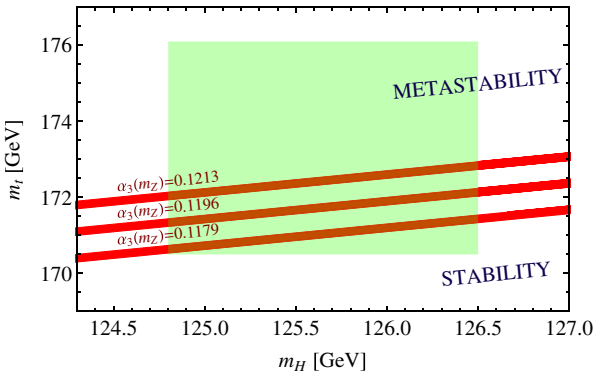

FIG. 6 (color online). The transition line between stability and metastability in the plane $[m_H, m_t]$ and for fixed values of $\alpha_3(m_Z) = 0.1196 \pm 0.0017$ [19]. The thickness of the lines represent the theoretical error due to the variation of μ_λ (the matching scale of λ) from m_Z up to $2m_H$. The shaded region is obtained by intersecting the 2σ ATLAS [1] and CMS [2] combined range ($m_H = 125.65 \pm 0.85$ GeV) with the running top mass range given by Ref. [15], $\bar{m}_t(m_t) = 163.3 \pm 2.7$ GeV, equivalent to $m_t = 173.3 \pm 2.8$ GeV.

[3]Of course, this assumes that the running of λ happens as in the SM up to energies close to the Planck scale without significant modifications.

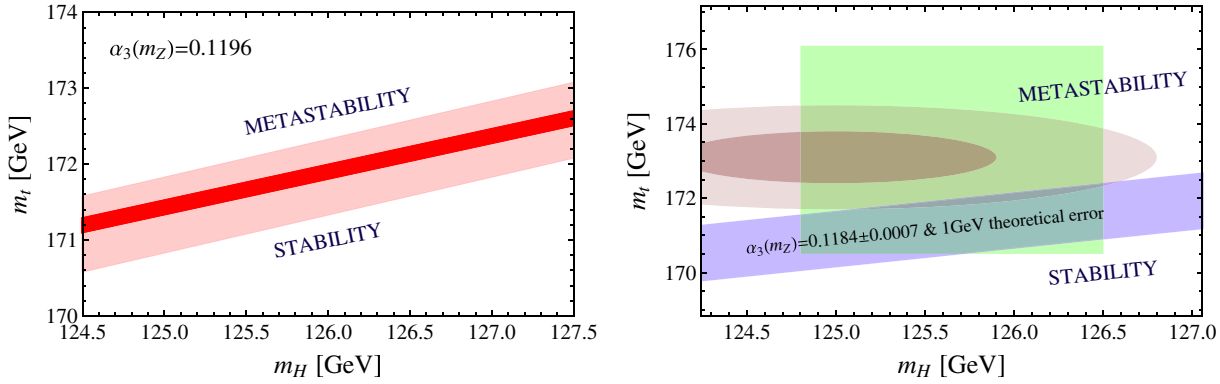

FIG. 7 (color online). Left: Theoretical uncertainty in the determination of the transition line between stability and metastability according to our Eq. (9) (thinner) and Eq. 10 of Ref. [14] (thicker). For definiteness we choose $\alpha_3(m_Z) = 0.1196$. Right: Transition line between stability and metastability according to Eq. 10 of Ref. [14]; the thickness of the band accounts for both the 1 GeV theoretical error and the experimental error due to the variation of $\alpha_3(m_Z)$ in the range 0.1184 ± 0.0007, as was done in Ref. [14]. The (brown) shaded disks represent the 1σ and 2σ combined ranges for m_t and m_H used in Ref. [14] (see their Fig. 5). The (green) rectangle allows for the comparison with the ranges of m_t and m_H used here (see Fig. 6).

Clearly, all these considerations do not justify the different conclusions of the two papers and rather show that the different conclusions must come from the different ranges used for the three most relevant parameters: m_t, m_H, and $\alpha_3(m_Z)$. In Ref. [14] it was assumed that $m_t = (173.1 \pm 0.7)$ GeV and $m_H = (125 \pm 1)$ GeV; these errors are further combined in quadrature and the 1σ and 2σ (brown) disks in the right plot of Fig. 7 are obtained. These disks have to be confronted with our (green) rectangular region, obtained by using $m_t = (173.3 \pm 2.8)$GeV, as suggested in Ref. [15], and $m_H = (125.65 \pm 0.85)$GeV, as suggested by combining the ATLAS [1] and CMS [2] ranges at 2σ. We have a rectangular region since we think that in this kind of analysis it is not really justified to combine in quadrature the errors on m_t and m_H, thus enhancing the exclusion of the interesting low-m_t and high-m_H values. A small value of $\alpha_3(m_Z)$ also goes in such a direction, since it lowers the transition line towards smaller values of m_t. In Ref. [14] it is assumed that $\alpha_3(m_Z) = 0.1184 \pm 0.0007$: the corresponding transition line is displayed in the right plot of Fig. 7, using Eq. (10) for consistency. The line perfectly reproduces the results of Fig. 5 of Ref. [14]; its thickness accounts for both the theoretical error and the experimental error due to the variation of $\alpha_3(m_Z)$, as derived in Ref. [14]. [We cannot display three separate lines, as done in Fig. 6, since in Eq. (10) the theoretical error and the error associated to the variation of $\alpha_3(m_Z)$ are comparable]. As the transition line marginally overlaps with the 2σ disk, the authors of Ref. [14] concluded that stability is disfavored. A very different conclusion would be derived by considering instead the broad overlap with the rectangle. This is the main reason for the different conclusions. A small role is also played by the different values used for $\alpha_3(m_Z)$. The range of $\alpha_3(m_Z)$ used in Ref. [14] has a very small error and has already been questioned in Ref. [15] (see bottom of p. 8). In the present analysis we instead use $\alpha_3(m_Z) = 0.1196 \pm 0.0017$ [19], whose central value and experimental error are bigger than those used in Ref. [14]. As an effect, the ensemble of the three (red) lines in Fig. 6 forms a band slightly wider and higher than the (blue) band in Fig. 7 that depicts the results of Ref. [14].

In summary, upon comparison of our results in Fig. 6 with the results of Ref. [14] reproduced in the right plot of Fig. 7, one can conclude that the difference in the physical interpretation of the results is mainly due to the fact that Ref. [14] adopted a too small experimental error for m_t, as was already pointed out in Ref. [15].

IV. SHALLOW FALSE MINIMUM

It is interesting to study in some detail the boundary conditions which must be satisfied in order to have a very shallow false minimum just below the Planck scale, since it could be relevant for inflation [7,17,18].

To study this particular configuration, we denote with μ_i the renormalization scale where the Higgs potential has an inflection point; we also recall that μ_β has been defined to be the scale where $\lambda(\mu_\beta) = 0$ and $\beta_\lambda(\mu_\beta) = 0$ are simultaneously fulfilled. Both μ_i and μ_β increase[4] with m_H, as shown in Fig. 8, where the shaded region accounts for the experimental range of $\alpha_3(m_Z)$.

It is interesting that, for the whole experimental range of m_H, a shallow false minimum is obtained only if the following boundary condition holds:

$$\lambda(\mu_\beta) \simeq (8.75 \pm 0.15) \times 10^{-6}. \tag{11}$$

One could speculate that such a value could originate from some quantum gravity effect [6,36]. In the left plot of Fig. 9 we show that $\lambda(\mu_\beta)$ has a mild dependence on

[4]Notice that μ_i is slightly smaller than μ_β. This can be easily understood, since the condition for having an inflection point at μ_i reads $\beta_\lambda(\mu_i) = -4\lambda(\mu_i) < 0$, which implies $\mu_i < \mu_\beta$.

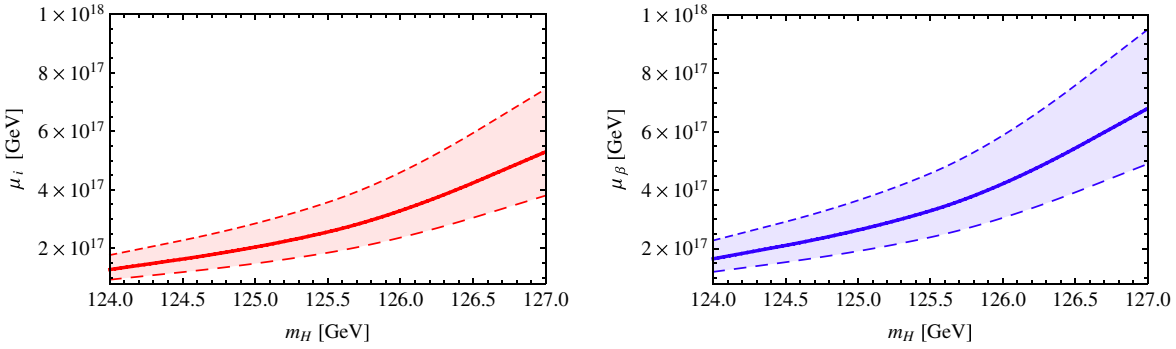

FIG. 8 (color online). Values of μ_i (left) and μ_β (right) as a function of m_H. For the solid lines, the input parameters are fixed at their central values and the matching of λ is done at $\mu = m_H$. The shaded regions show the uncertainty induced by the experimental error of $\alpha_3(m_Z) = 0.1196 \pm 0.0017$: the short and long dashed curves refer to the lower and upper value at 1σ, respectively.

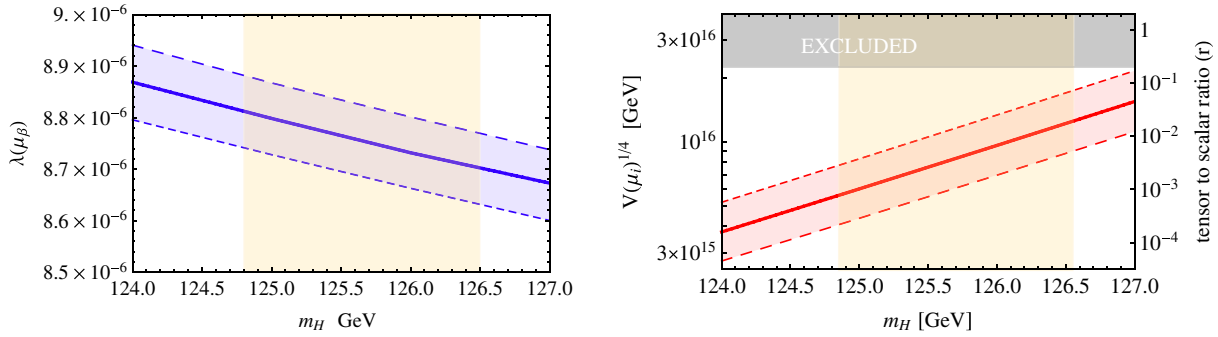

FIG. 9 (color online). Left: The value of $\lambda(\mu_\beta)$ as a function of m_H. Right: The Higgs potential at μ_i and the associated prediction for r as a function of m_H. The short and long dashed curves refer to the 1σ lower and upper values of $\alpha_3(m_Z)$, respectively. The shaded (yellow) vertical region marks the preferred range of m_H at 2σ [1,2]. The upper region in the right plot is excluded because $r \lesssim 0.2$ [37].

m_H; in the right plot we show instead the value of the Higgs potential at the inflection point, which turns out to be of $\mathcal{O}(10^{16})$ GeV. As before, the shaded regions account for the experimental range of $\alpha_3(m_Z)$.

As pointed out in Ref. [17], a way of testing the hypothesis that inflation occurred when the Higgs field was trapped into a shallow false vacuum below the Planck scale is to look at the tensor-to-scalar ratio r of cosmological perturbations. The amplitude of the density fluctuations in the observed Universe as seen by the CMB and large-scale structure data is parametrized by the power spectrum in k space, $P_s(k) = \Delta_R^2 (k/k_0)^{n_s - 1}$, where Δ_R^2 is the amplitude at some pivot point k_0, whose best-fit value is $\Delta_R^2 = (2.43 \pm 0.11) \times 10^{-9}$ at $k_0 = 0.002$ Mpc^{-1} [37]. In models where inflation happened while the Higgs was trapped in the shallow minimum [7,18], the Higgs potential at the inflection point and the amount of gravity waves that can be produced—parametrized via the tensor-to-scalar ratio r—are linked via a simple relation,

$$\Delta_R^2 = \frac{2}{3\pi^2} \frac{1}{r} \frac{V(\mu_i)}{M^4}, \tag{12}$$

where M is the reduced Planck scale. Such a prediction for r is reported in the right plot of Fig. 9. Notice that, for these models, only when m_H is in its upper allowed range and $\alpha_3(m_Z)$ is quite low is there a chance for the Planck satellite mission [38] to measure r. However, the forthcoming experiment EPIC [39] should be able to test r down to 10^{-2}, while COrE [40] should be able to test down to about 10^{-3}.

V. CONSTRAINTS ON THE SEESAW MECHANISM

We now consider the effect of including neutrino masses via a type-I seesaw. This issue has already been considered in a series of papers [8,41–44].

Although the precise amount of the effect is quite model dependent, here we obtain a conservative estimate of the effect by considering only one right-handed neutrino with mass M_ν, associated to a light Majorana neutrino with mass $m_\nu = 0.06$ eV, which is the scale of the atmospheric oscillations. This is supported by the following argument.

It is well known that the β function of the Higgs quartic coupling is affected only if $h_\nu(\mu)$, the Yukawa coupling of the Dirac mass term (defined only for $\mu \geq M_\nu$), is large enough. Similar to the top Yukawa coupling, the neutrino Yukawa coupling induces a suppression of the Higgs quartic coupling at high energy. By increasing M_ν and m_ν, the neutrino Yukawa coupling at the threshold scale M_ν also increases,

$$h_\nu(M_\nu) = 2\sqrt{\frac{m_\nu(M_\nu)M_\nu}{v^2}}. \quad (13)$$

This justifies the fact that we equate m_ν to the the atmospheric mass scale of about 0.06 eV, which is the lowest possible value for the heaviest among the three light neutrinos. In addition, two other Majorana neutrinos with masses lighter than m_ν can be accommodated via the seesaw, but if their right-handed neutrinos are lighter than M_ν the associated Dirac Yukawa couplings are naturally expected to be smaller, and their effect on $\lambda(\mu)$ would be negligible.

In Appendix B we provide the additional terms (with respect to the pure SM) for the relevant β functions, above and below the scale M_ν.

Since the effect of h_ν is a suppression of λ, an SM configuration with a stable electroweak vacuum could be rendered metastable because of the addition of the seesaw interactions. For a fixed value of m_H, and in the range of the top-mass values allowing the electroweak vacuum to be the global one, one can find the upper bound on M_ν from the requirement that the electroweak vacuum remains the global one even after the inclusion of the seesaw interactions. Clearly, such an upper limit cannot be derived in the range of the top-mass values for which the electroweak vacuum is already metastable. As shown in Fig. 10 for $m_H = 126$ GeV (but similar upper bounds are obtained in the whole experimental range of m_H), such an upper bound strongly depends on the top mass[5] and is affected by an uncertainty that is mainly due to $\alpha_3(m_Z)$ (shaded region). As the top mass decreases, the configuration of the Higgs potential becomes more stable and the M_ν upper bound that ensures that the electroweak vacuum remains the global one and does not become metastable becomes less stringent: $M_\nu \lesssim 3 \times 10^{14}$ GeV. However, by increasing the top mass the electroweak vacuum becomes less stable and the upper bound on M_ν becomes accordingly more and more stringent. Increasing the top mass further causes the electroweak vacuum to become metastable even without seesaw interactions, so that no meaningful bound can be derived.

The upper bound on M_ν following from the requirement of electroweak vacuum stability has to be taken *cum grano salis*, in the sense that it is not a physically robust bound, but rather just a bound that should be respected in the case that one has a model in which the Higgs potential has to remain stable for some reason.

We consider in particular the upper bound on M_ν needed to avoid the destabilization of an inflection-point configuration, such as the one depicted via the dashed line in Fig. 11. Notice that an inflection point becomes a not-so-shallow local second minimum if $M_\nu \sim 10^{11}$ GeV and that

[5]This dependence was not considered in the previous literature.

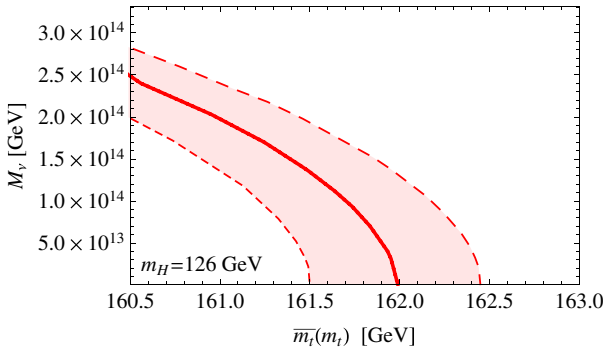

FIG. 10 (color online). Upper bound on M_ν as a function of the running top mass, following from the requirement that the electroweak vacuum is not destabilized because of the inclusion of the seesaw, for $m_H = 126$ GeV. The shaded region is obtained by varying $\alpha_3(m_Z)$ in its 1σ range.

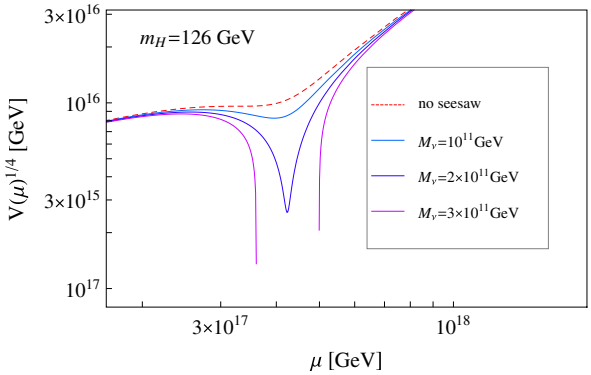

FIG. 11 (color online). The dashed curve represents the Higgs potential as a function of the renormalization scale, for $m_H = 126$ GeV, $\alpha_3(m_Z) = 0.1196$, and $m_t = 171.56$ GeV (the value of the top mass leading to an inflection-point configuration in the SM case with the former two parameters fixed). The solid lower curves display the effect of adding the seesaw, with three increasing values of M_ν from top to bottom.

electroweak vacuum destabilization is avoided only if the condition $M_\nu \lesssim 2 \times 10^{11}$ GeV is satisfied. The latter bound might be relevant for models of inflation based on the SM shallow false minimum [7,17,18]; note however that it is well compatible with the thermal leptogenesis mechanism used to explain the matter-antimatter asymmetry, for which the lower bound on the lightest Majorana neutrino is about 5×10^8 GeV [45].

Clearly, the neutrino Yukawa coupling y_ν is not the only additional term beyond the SM capable of modifying the running of λ at high energy. As always in the context of a type-I seesaw, in the case that the vacuum expectation value of a singlet scalar field S (violating the lepton number by two units) is actually at the origin of the right-handed Majorana neutrino mass, the S couplings induce an enhancement of λ, thus helping the stability of the electroweak vacuum [46]. Such an effect is indeed generically expected when adding a singlet field S to the SM [46,47].

VI. CONCLUSIONS

The recent discovery of a particle consistent with the SM Higgs boson [1,2] provides a strong motivation to pursue [6–9,13–15,17] the old project [3–5] of investigating the behavior of the SM Higgs potential at very high energies. In particular, one should understand whether the SM electroweak vacuum is a global minimum up to the Planck scale, namely, whether we live in a stable vacuum assuming a desert (or assuming that new interactions do not modify the running of λ with respect to the SM case). In particular, a stable configuration that deserves special attention is a shallow false minimum below the Planck scale; the Higgs field could have been primordially trapped there, leading to a stage of inflation [7,17,18]. Stability below the Planck scale is also required in Higgs inflation models with nonminimal gravitational couplings [13,48].

In our analysis, we adopted the recently derived tools for an NNLO renormalization procedure [11–14]. As opposed to previous analyses, we considered as a free parameter the running top mass rather than the (Tevatron) top pole mass, as suggested in Ref. [15].

Given the present range of the running top mass and of the Higgs mass, we found that electroweak vacuum stability is at present allowed, as shown in Figs. 5 and 6. To further test stability, a more precise measurement of the top mass is crucial. As is apparent from the stability condition of Eq. (9), in the case that the LHC will not exclude values of the running top mass below 163 GeV (or, equivalently, values of the top pole mass below 173 GeV), an electron-positron collider would probably be needed to discriminate between stability and metastability.

We also determined the high-scale boundary conditions that allow for a shallow false minimum slightly below the Planck scale, $\lambda(\mu_\beta) \sim 10^{-5}$ (μ_β is the renormalization scale where the β function of the Higgs quartic coupling vanishes), and discussed the prospects for cosmological tests of such a configuration. Finally, a conservative upper bound on type-I seesaw right-handed neutrino masses, following from the requirement of electroweak vacuum stability, was derived, and its dependence on the top mass was analyzed.

The present analysis does not consider the effect of the gravitational couplings because it is far from clear how the quantum effects of the latter would impact studies at very high energies. Other sources of uncertainty could also come from the treatment of the effective potential itself, such as the fine-tuning required for both the cosmological constant and the Higgs mass.

ACKNOWLEDGMENTS

We would like to thank G. Isidori, G. Moore, A. Notari, and A. Strumia for useful discussions.

APPENDIX A: FORMULAS FOR THE RG RUNNING AT NNLO

1. The β functions

Here we provide the expressions for the β functions up to three loops; see Eq. (2).
At the one-loop level they are given by

$$\beta_\lambda^{(1)} = \frac{27}{4}g(t)^4 + \frac{9}{2}g'(t)^2 g(t)^2 - 9\lambda(t)g(t)^2 + \frac{9}{4}g'(t)^4 - 36h_t(t)^4 + 4\lambda(t)^2 - 3g'(t)^2\lambda(t) + 12h_t(t)^2\lambda(t),$$

$$\beta_{h_t}^{(1)} = \frac{9}{2}h_t(t)^3 - \frac{9}{4}g(t)^2 h_t(t) - 8g_3(t)^2 h_t(t) - \frac{17}{12}g'(t)^2 h_t(t), \qquad \beta_g^{(1)} = -\frac{19}{6}g(t)^3, \qquad \beta_{g'}^{(1)} = \frac{41}{6}g'(t)^3,$$

$$\beta_{g_3}^{(1)} = -7g_3(t)^3.$$

At the two-loop level they are

$$\begin{aligned}\beta_\lambda^{(2)} = {} & 80g_3(t)^2 h_t(t)^2\lambda(t) - 192g_3(t)^2 h_t(t)^4 + \frac{915}{8}g(t)^6 - \frac{289}{8}g'(t)^2 g(t)^4 - \frac{27}{2}h_t(t)^2 g(t)^4 - \frac{73}{8}\lambda(t)g(t)^4 \\ & - \frac{559}{8}g'(t)^4 g(t)^2 + 63g'(t)^2 h_t(t)^2 g(t)^2 + \frac{39}{4}g'(t)^2\lambda(t)g(t)^2 - 3h_t(t)^4\lambda(t) + \frac{45}{2}h_t(t)^2\lambda(t)g(t)^2 - \frac{379}{8}g'(t)^6 \\ & + 180h_t(t)^6 - 16g'(t)^2 h_t(t)^4 - \frac{26}{3}\lambda(t)^3 - \frac{57}{2}g'(t)^4 h_t(t)^2 - 24h_t(t)^2\lambda(t)^2 + 6(3g(t)^2 + g'(t)^2)\lambda(t)^2 \\ & + \frac{629}{24}g'(t)^4\lambda(t) + \frac{85}{6}g'(t)^2 h_t(t)^2\lambda(t),\end{aligned}$$

$$\begin{aligned}\beta_{h_t}^{(2)} = {} & h_t(t)\Big[-108g_3(t)^4 + 9g(t)^2 g_3(t)^2 + \frac{19}{9}g'(t)^2 g_3(t)^2 + 36h_t(t)^2 g_3(t)^2 - \frac{3}{4}g'(t)^2 g(t)^2 - \frac{23}{4}g(t)^4 + \frac{1187}{216}g'(t)^4 \\ & - 12h_t(t)^4 + \frac{\lambda(t)^2}{6} + h_t(t)^2\Big(\frac{225}{16}g(t)^2 + \frac{131}{16}g'(t)^2 - 2\lambda(t)\Big)\Big],\end{aligned}$$

$$\beta_g^{(2)} = 12 g_3(t)^2 g(t)^3 + \left(\frac{35}{6} g(t)^2 + \frac{3}{2} g'(t)^2 - \frac{3}{2} h_t(t)^2\right) g(t)^3,$$
$$\beta_{g'}^{(2)} = \frac{44}{3} g_3(t)^2 g'(t)^3 + \left(\frac{9}{2} g(t)^2 + \frac{199}{18} g'(t)^2 - \frac{17}{6} h_t(t)^2\right) g'(t)^3,$$
$$\beta_{g_3}^{(2)} = g_3(t)^3 \left(\frac{9}{2} g(t)^2 - 26 g_3(t)^2 + \frac{11}{6} g'(t)^2 - 2 h_t(t)^2\right).$$

The leading terms in the three-loop β functions of λ and h_t are [12]

$$\begin{aligned}\beta_\lambda^{(3)} = 12\Bigg[&\left(-\frac{266}{3} + 32\zeta_3\right) g_3(t)^4 h_t(t)^4 + (-38 + 240\zeta_3) g_3(t)^2 h_t(t)^6 - \left(\frac{1599}{8} + 36\zeta_3\right) h_t(t)^8 \\ &+ \frac{1}{6}\left(\frac{1244}{3} - 48\zeta_3\right) g_3(t)^4 h_t(t)^2 \lambda(t) + \frac{1}{6}(895 - 1296\zeta_3) g_3(t)^2 h_t(t)^4 \lambda(t) + \frac{1}{6}\left(\frac{117}{8} - 198\zeta_3\right) h_t(t)^6 \lambda(t) \\ &+ \frac{1}{36}(-1224 + 1152\zeta_3) g_3(t)^2 h_t(t)^2 \lambda(t)^2 + \frac{1}{36}\left(\frac{1719}{2} + 756\zeta_3\right) h_t(t)^4 \lambda(t)^2 \\ &+ \frac{97}{24} h_t(t)^2 \lambda(t)^3 + \frac{1}{1296}(3588 + 2016\zeta_3) \lambda(t)^4\Bigg],\end{aligned}$$
$$\begin{aligned}\beta_{h_t}^{(3)} = 2\Bigg[&\left(-\frac{2083}{3} + 320\zeta_3\right) g_3(t)^6 + \left(\frac{3827}{12} - 114\zeta_3\right) g_3(t)^4 h_t(t)^2 - \frac{157}{2} g_3(t)^2 h_t(t)^4 + \left(\frac{339}{16} + \frac{27}{4}\zeta_3\right) h(t)^6 \\ &+ \frac{4}{3} g_3(t)^2 h_t(t)^2 \lambda(t) + \frac{33}{2} h_t(t)^4 \lambda(t) + \frac{5}{96} h_t(t)^2 \lambda(t)^2 - \frac{1}{12} \lambda(t)^3\Bigg],\end{aligned}$$

where $\zeta_3 = 1.20206\ldots$ is the Riemann zeta function.

The complete three-loop β functions for the gauge couplings are [11]

$$\begin{aligned}\beta_g^{(3)} = &\frac{324953}{1728} g(t)^7 + 39 g(t)^5 g_3(t)^2 + 81 g(t)^3 g_3(t)^4 + \frac{291}{32} g(t)^5 g'(t)^2 - \frac{1}{3} g(t)^3 g_3(t)^2 g'(t)^2 - \frac{5597}{576} g(t)^3 g'(t)^4 \\ &- \frac{729}{32} g(t)^5 h_t(t)^2 - 7 g(t)^3 g_3(t)^2 h_t(t)^2 - \frac{593}{96} g(t)^3 g'(t)^2 h_t(t)^2 + \frac{147}{16} g(t)^3 h_t(t)^4,\end{aligned}$$
$$\begin{aligned}\beta_{g'}^{(3)} = &\frac{1315}{64} g(t)^4 g'(t)^3 - g(t)^2 g_3(t)^2 g'(t)^3 + 99 g_3(t)^4 g'(t)^3 + \frac{205}{96} g(t)^2 g'(t)^5 - \frac{137}{27} g_3(t)^2 g'(t)^5 - \frac{388613}{5184} g'(t)^7 \\ &- \frac{785}{32} g(t)^2 g'(t)^3 h_t(t)^2 - \frac{29}{3} g_3(t)^2 g'(t)^3 h_t(t)^2 - \frac{2827}{288} g'(t)^5 h_t(t)^2 + \frac{315}{16} g'(t)^3 h_t(t)^4,\end{aligned}$$
$$\begin{aligned}\beta_{g_3}^{(3)} = &\frac{109}{8} g(t)^4 g_3(t)^3 + 21 g(t)^2 g_3(t)^5 + \frac{65}{2} g_3(t)^7 - \frac{1}{8} g(t)^2 g_3(t)^3 g'(t)^2 + \frac{77}{9} g_3(t)^5 g'(t)^2 - \frac{2615}{216} g_3(t)^3 g'(t)^4 \\ &- \frac{93}{8} g(t)^2 g_3(t)^3 h_t(t)^2 - 40 g_3(t)^5 h_t(t)^2 + \frac{101}{24} g_3(t)^3 g'(t)^2 h_t(t)^2 + 15 g_3(t)^3 h_t(t)^4.\end{aligned}$$

2. Higgs quartic coupling matching

According to Sirlin and Zucchini [27], the one-loop matching is given by

$$\delta_H^{(1)}(\mu) = \frac{G_\mu m_Z^2}{8\sqrt{2}\pi^2}\left(\xi f_1(\mu) + f_0(\mu) + \frac{f_{-1}(\mu)}{\xi}\right),$$

where $\xi = \frac{m_H^2}{m_Z^2}$ and, introducing $c = \frac{m_W}{m_Z}$,

$$f_1(\mu) = \frac{3}{2}\log(\xi) - \log(c^2) + 6\log\left(\frac{\mu^2}{m_H^2}\right) - \frac{1}{2}Z\left[\frac{1}{\xi}\right] - Z\left[\frac{c^2}{\xi}\right] + \frac{9}{2}\left(\frac{25}{9} - \frac{\pi}{\sqrt{3}}\right),$$

$$f_0(\mu) = \frac{3c^2}{s^2}\log(c^2) + 12\log c^2(c^2) + \frac{3\xi c^2}{\xi - c^2}\log\left(\frac{\xi}{c^2}\right) + 4c^2 Z\left[\frac{c^2}{\xi}\right] - \frac{15}{2}(2c^2+1) - 6\left(2c^2 - \frac{2m_t^2}{m_Z^2} + 1\right)\log\left(\frac{\mu^2}{m_Z^2}\right)$$
$$- \frac{3m_t^2}{m_Z^2}\left(4\log\left(\frac{m_t^2}{m_Z^2}\right) + 2Z\left[\frac{m_t^2}{m_Z^2\xi}\right] - 5\right) + 2Z\left[\frac{1}{\xi}\right],$$

$$f_{-1}(\mu) = 8(2c^4+1) - 12c^4\log(c^2) - 12c^4 Z\left[\frac{c^2}{\xi}\right] + 6\left(2c^4 - \frac{4m_t^4}{m_Z^4} + 1\right)\log\left(\frac{\mu^2}{m_Z^2}\right)$$
$$- 6Z\left[\frac{1}{\xi}\right] + \frac{24m_t^4}{m_Z^4}\left(\log\left(\frac{m_t^2}{m_Z^2}\right) + Z\left[\frac{m_t^2}{m_Z^2\xi}\right] - 2\right),$$

$$Z[z] = \begin{cases} 2A(z)\arctan\left(\frac{1}{A(z)}\right) & \text{if } z > \frac{1}{4} \\ A(z)\log\left(\frac{A(z)+1}{1-A(z)}\right) & \text{if } z < \frac{1}{4} \end{cases}, \qquad A(z) = \sqrt{|1-4z|}.$$

We compute the QCD and Yukawa contributions to $\lambda^{(2)}(\mu)$ following the expressions of Ref. [14] (multiplying them by a factor of 6 to compensate for the different definition of the quartic coupling).

APPENDIX B: SEESAW CONTRIBUTION TO THE β FUNCTIONS

Below the right-handed neutrino mass scale, the running of the effective light Majorana neutrino mass is given by [49]

$$\frac{dm_\nu(t)}{dt} = \kappa\left(-3g_2(t)^2 + 6h_t(t)^2 + \frac{\lambda(t)}{6}\right)m_\nu(t).$$

For $\mu > M_\nu$, we have [50]

$$\frac{dh_\nu(t)}{dt} = \kappa h_\nu(t)\left(\frac{5}{4}h_\nu(t)^2 + \frac{3}{2}h_t(t)^2 - \frac{3}{4}g'(t)^2 - \frac{9}{4}g(t)^2\right),$$

together with

$$\delta\beta_\lambda^{(1)} = -3h_\nu(t)^4 + 2\lambda(t)h_\nu(t)^2, \qquad \delta\beta_{h_t}^{(1)} = \frac{1}{2}h_\nu(t)^2.$$

[1] The ATLAS Collaboration, Phys. Lett. B **716**, 1 (2012).
[2] The CMS Collaboration, Phys. Lett. B **716**, 30 (2012).
[3] P. Q. Hung, Phys. Rev. Lett. **42**, 873 (1979); N. Cabibbo, L. Maiani, G. Parisi, and R. Petronzio, Nucl. Phys. **B158**, 295 (1979); M. Lindner, Z. Phys. C **31**, 295 (1986); M. Lindner, M. Sher, and H. W. Zaglauer, Phys. Lett. B **228**, 139 (1989); M. Sher, Phys. Rep. **179**, 273 (1989); M. Sher, Phys. Lett. B **317**, 159 (1993); Phys. Lett. B **331**, 448(E) (1994); G. Altarelli and G. Isidori, Phys. Lett. B **337**, 141 (1994); C. D. Froggatt and H. B. Nielsen, Phys. Lett. B **368**, 96 (1996); B. Schrempp and M. Wimmer, Prog. Part. Nucl. Phys. **37**, 1 (1996).
[4] J. A. Casas, J. R. Espinosa, and M. Quiros, Phys. Lett. B **342**, 171 (1995); J. R. Espinosa and M. Quiros, Phys. Lett. B **353**, 257 (1995); J. A. Casas, J. R. Espinosa, and M. Quiros, Phys. Lett. B **382**, 374 (1996).
[5] G. Isidori, G. Ridolfi, and A. Strumia, Nucl. Phys. **B609**, 387 (2001); J. R. Espinosa, G. F. Giudice, and A. Riotto, J. Cosmol. Astropart. Phys. 05 (2008) 002; G. Isidori, V. S. Rychkov, A. Strumia, and N. Tetradis, Phys. Rev. D **77**, 025034 (2008); N. Arkani-Hamed, S. Dubovsky, L. Senatore, and G. Villadoro, J. High Energy Phys. 03 (**2008**) 075; J. Ellis, J. R. Espinosa, G. F. Giudice, A. Hoecker, and A. Riotto, Phys. Lett. B **679**, 369 (2009).
[6] M. Holthausen, K. S. Lim, and M. Lindner, J. High Energy Phys. 02 (2012) 037.
[7] I. Masina and A. Notari, Phys. Rev. D **85**, 123506 (2012).
[8] J. Elias-Miro, J. R. Espinosa, G. F. Giudice, G. Isidori, A. Riotto, and A. Strumia, Phys. Lett. B **709**, 222 (2012).
[9] Z.-z. Xing, H. Zhang, and S. Zhou, Phys. Rev. D **86**, 013013 (2012).
[10] ATLAS Collaboration, Phys. Lett. B **710**, 49 (2012); ATLAS Collaboration Phys. Rev. Lett. **108**, 111803 (2012); ATLAS Collaboration Phys. Lett. B **710**, 383 (2012); CMS Collaboration, Phys. Lett. B **710**, 26 (2012).
[11] L. N. Mihaila, J. Salomon, and M. Steinhauser, Phys. Rev. Lett. **108**, 151602 (2012).
[12] K. G. Chetyrkin and M. F. Zoller, J. High Energy Phys. 06 (2012) 033.
[13] F. Bezrukov, M. Y. Kalmykov, B. A. Kniehl, and M. Shaposhnikov, J. High Energy Phys. 10 (2012) 140.
[14] G. Degrassi, S. Di Vita, J. Elias-Miro, J. R. Espinosa, G. F. Giudice, G. Isidori, and A. Strumia, J. High Energy Phys. 08 (2012) 098.

[15] S. Alekhin, A. Djouadi, and S. Moch, Phys. Lett. B **716**, 214 (2012).

[16] Tevatron Electroweak Working Group, CDF, and D0 Collaborations, arXiv:1107.5255.

[17] I. Masina and A. Notari, Phys. Rev. Lett. **108**, 191302 (2012).

[18] I. Masina and A. Notari, J. Cosmol. Astropart. Phys. 11 (2012) 031.

[19] J. Beringer *et al.* (Particle Data Group), Phys. Rev. D **86**, 010001 (2012).

[20] C. Ford, D. R. T. Jones, P. W. Stephenson, and M. B. Einhorn, Nucl. Phys. **B395**, 17 (1993); C. Ford, I. Jack, and D. R. T. Jones, Nucl. Phys. **B387**, 373 (1992); **B504**, 551(E) (1997).

[21] D. J. Gross and F. Wilczek, Phys. Rev. Lett. **30**, 1343 (1973); Phys. Rev. D **8**, 3633 (1973); H. D. Politzer, Phys. Rev. Lett. **30**, 1346 (1973); D. R. T. Jones, Nucl. Phys. **B75**, 531 (1974); W. E. Caswell, Phys. Rev. Lett. **33**, 244 (1974).

[22] O. V. Tarasov and A. A. Vladimirov, Yad. Fiz. **25**, 1104 (1977) [Sov. J. Nucl. Phys. **25**, 585 (1977)]; O. V. Tarasov, A. A. Vladimirov, and A. Y. Zharkov, Phys. Lett. **93B**, 429 (1980); D. R. T. Jones, M. Fischler, and J. Oliensis, Phys. Lett. **119B**, 385 (1982); M. E. Machacek and M. T. Vaughn, Nucl. Phys. **B222**, 83 (1983); **B236**, 221 (1984); **B249**, 70 (1985).

[23] S. A. Larin and J. A. M. Vermaseren, Phys. Lett. B **303**, 334 (1993).

[24] T. van Ritbergen, J. A. M. Vermaseren, and S. A. Larin, Phys. Lett. B **400**, 379 (1997).

[25] M.-x. Luo and Y. Xiao, Phys. Rev. Lett. **90**, 011601 (2003).

[26] M. Czakon, Nucl. Phys. **B710**, 485 (2005).

[27] A. Sirlin and R. Zucchini, Nucl. Phys. **B266**, 389 (1986).

[28] R. Hempfling and B. A. Kniehl, Phys. Rev. D **51**, 1386 (1995).

[29] K. G. Chetyrkin and M. Steinhauser, Nucl. Phys. **B573**, 617 (2000).

[30] N. Gray, D. J. Broadhurst, W. Grafe, and K. Schilcher, Z. Phys. C **48**, 673 (1990).

[31] D. J. Broadhurst, N. Gray, and K. Schilcher, Z. Phys. C **52**, 111 (1991).

[32] J. Fleischer, F. Jegerlehner, O. V. Tarasov, and O. L. Veretin, Nucl. Phys. **B539**, 671 (1999); **B571**, 511(E) (2000).

[33] K. Melnikov and T. v. Ritbergen, Phys. Lett. B **482**, 99 (2000).

[34] F. Jegerlehner and M. Y. Kalmykov, Nucl. Phys. **B676**, 365 (2004).

[35] The ATLAS Collaboration, arXiv:0901.0512; The CMS Collaboration, J. Phys. G **34**, 995 (2007).

[36] M. Shaposhnikov and C. Wetterich, Phys. Lett. B **683**, 196 (2010).

[37] E. Komatsu *et al.* (WMAP Collaboration), Astrophys. J. Suppl. Ser. **192**, 18 (2011).

[38] The Planck Collaboration, arXiv:astro-ph/0604069; See also C. Burigana, C. Destri, H. J. de Vega, A. Gruppuso, N. Mandolesi, P. Natoli, and N. G. Sanchez, Astrophys. J. **724**, 588 (2010).

[39] J. Bock *et al.* (EPIC Collaboration), arXiv:0906.1188.

[40] The COrE Collaboration, arXiv:1102.2181.

[41] J. A. Casas, V. Di Clemente, A. Ibarra, and M. Quiros, Phys. Rev. D **62**, 053005 (2000).

[42] I. Gogoladze, N. Okada, and Q. Shafi, Phys. Lett. B **668**, 121 (2008).

[43] W. Rodejohann and H. Zhang, J. High Energy Phys. 06 (2012) 022.

[44] J. Chakrabortty, M. Das, and S. Mohanty, arXiv:1207.2027.

[45] S. Davidson and A. Ibarra, Phys. Lett. B **535**, 25 (2002).

[46] J. Elias-Miro, J. R. Espinosa, G. F. Giudice, H. M. Lee, and A. Strumia, J. High Energy Phys. 06 (2012) 031; See also L. Basso, S. Moretti, and G. M. Pruna, Phys. Rev. D **82**, 055018 (2010).

[47] O. Lebedev, Eur. Phys. J. C **72**, 2058 (2012).

[48] F. L. Bezrukov and M. Shaposhnikov, Phys. Lett. B **659**, 703 (2008); J. High Energy Phys. 07 (2009) 089; F. Bezrukov, D. Gorbunov, and M. Shaposhnikov, J. Cosmol. Astropart. Phys. 10 (2011) 001; For a classification of models with nonminimal couplings, see K. Kamada, T. Kobayashi, T. Takahashi, M. Yamaguchi, and J. 'i. Yokoyama, Phys. Rev. D **86**, 023504 (2012).

[49] K. S. Babu, C. N. Leung, and J. T. Pantaleone, Phys. Lett. B **319**, 191 (1993).

[50] Y. F. Pirogov and O. V. Zenin, Eur. Phys. J. C **10**, 629 (1999).